Design of a smart MEMS accelerometer using nonlinear control principles

Faezeh Arab Hassani[†], Amir Farrokh Payam[‡] and Morteza Fathipour[*]

Device Simulation and Modeling Laboratory, Faculty of Electrical and Computer Engineering, Campus #2, University of Tehran, North Kargar St., P.O.BOX 14395-515, Tehran, Iran

Abstract. This paper presents a novel smart MEMS accelerometer which employs a hybrid control algorithm and an estimator. This scheme is realized by adding a sliding-mode controller to a conventional PID closed loop system to achieve higher stability and higher dynamic range and to prevent pull-in phenomena by preventing finger displacement from passing a maximum preset value as well as adding an adaptive nonlinear observer to a conventional PID closed loop system. This estimator is used for online estimation of the parameter variations for MEMS accelerometers and gives the capability of self testing to the system. The analysis of convergence and resolution show that while the proposed control scheme satisfies these criteria it also keeps resolution performance better than what is normally obtained in conventional PID controllers. The performance of the proposed hybrid controller investigated here is validated by computer simulation.

Keywords: Micro Electromechanical Systems (MEMS); pull-in phenomena; PID closed loop system; sliding-mode controller; adaptive nonlinear observer.

1. Introduction

Micro Electromechanical Systems (MEMS) contain extremely small mechanical elements, often integrated together with electronic processing circuitry. One of the most important categories of these micro devices is MEMS accelerometer (SPC 1994). While significant research has been focused on the design and fabrication of the MEMS accelerometers (Zhang 1998, Yazdi, *et al.* 1998, Vishal 2000), studies on the control of these systems are limited. The theory of nonlinear, robust and adaptive control has been extensively explained in numerous references (Edvards and Spurgeon 1998, Krstic, *et al.* 1995, Slotine and Jacques 1991, Spooner, *et al.* 2002). These controllers have many advantages such as fast dynamic response, robustness, higher efficiency, etc. Application of nonlinear control in electromechanical systems has attracted considerable interest in recent years. These techniques have recently been considered to control electrostatic MEMS structures in order to extend the stable operational range, minimize sensitivity and to improve the overall systems performance (Lyshvitz and Lyshvitz 2000, Zhu, *et al.* 2006, Park and Horowitz 2003).

In this paper a smart MEMS accelerometer which consists of combination of hybrid controller and an

[†]E-mail: faezeh.arabhassani@gmail.com
[‡]E-mail: amir_farokh@yahoo.com
[*]Corresponding author, E-mail: mfathi@ut.ac.ir

estimator for a capacitive MEMS accelerometer is designed based on sliding-mode and adaptive input-output feedback linearization principles (Spooner, *et al.* 2002). This method not only allows detection of the spring stiffness and the damping factor of the MEMS accelerometer in an online fashion but also provides the capability of self testing. Furthermore it allows achieving higher stability and dynamic range and prevents occurrence of pull-in phenomena. Accurate determination of the pull-in voltage is critical in the sensor or actuator design process to determine the sensitivity, frequency response, distortion and the dynamic range of the device (Chowdhury, *et al.* 2005). Adding the hybrid control system not only provides a self test system but also prevents the unwanted pull-in phenomenon. One of the most important characteristics of the present estimator is the ability to either work with or without feedback controller for MEMS accelerometer. Simulation results, confirm the effectiveness and improved performance of this designed MEMS accelerometer. In section 2 the design of accelerometer is presented. In section 3 we explain the open and closed loop controllers for the MEMS capacitive accelerometers. The PID controller for the accelerometer is described in section 4. In section 5 the sliding mode controller is described and the sliding-mode design of closed loop system is considered in section 6. In section 7 the adaptive nonlinear observer is described while in section 8 design process for an observer based on adaptive input-output feedback linearization principle for the desired accelerometer is explained.

2. The accelerometer design

In Fig. 1(a) the movable part of the y-axis accelerometer structure and in Fig. 1(b), the magnified part of the accelerometer are shown. Several fixed fingers are also shown in Fig. 1(b) in order to represent the gap between the movable and fixed fingers (g_0). We assume that the accelerometer is fabricated using polysilicon surface micromachining and the whole released structure is uniform with a constant thickness (H). We consider two main factors for design namely maximum acceleration (a_{max}) and noise density aside from the dimensions (i.e. g_0) that are set by the fabrication technology. The accelerometer operates in an under damped mode with a quality factor of 2 to ensure both a low noise floor and fast settling time. To ensure stable operation of the accelerometer the maximum displacement (x_{max}) is set equal to $0.2g_0$ in (Lobontiu and Garcia 2005). The resonance frequency is thus obtained from:
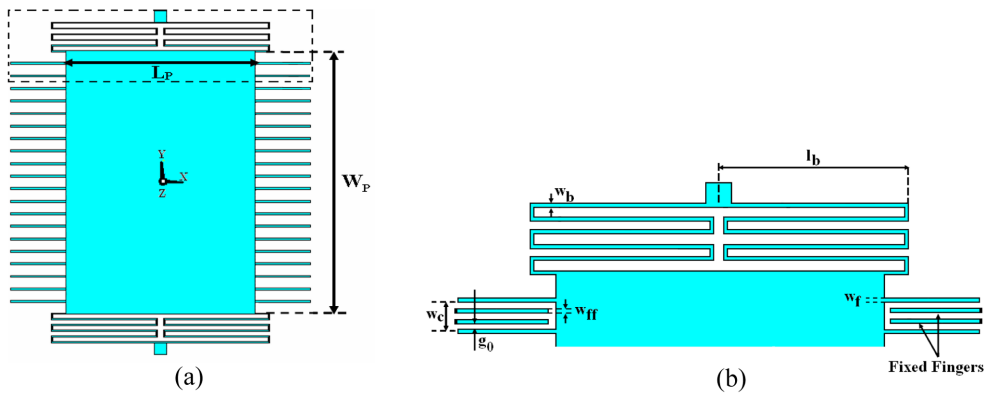

Fig. 1 (a) The y-axis accelerometer structure (b) The magnified part of the accelerometer and the added fixed fingers

$$\omega_r = \sqrt{\frac{a}{x}} \tag{1}$$

The minimum value for mass (m_1) is given by (Luo, *et al.* 2002):

$$m_1 = \frac{4k_B T \omega_r}{Q \frac{a^2}{\Delta f}} \tag{2}$$

Where Q is quality factor, T is temperature, $a/\sqrt{\Delta f}$ is the noise density and k_B is the Boltzman constant. In order to keep reliable confidence margin for sensitivity, Signal to Noise Ratio (SNR) is assumed to be 25. Mass is described as:

$$m = SNR m_1 \tag{3}$$

Damping factor (b) is described by:

$$b = \frac{m \omega_r}{Q} \tag{4}$$

Spring stiffness (k) is given by:

$$k = m \omega_r^2 \tag{5}$$

If we assume viscous flow between parallel plates and squeeze film damping, b is estimated as:

$$b = \mu A_s \left(\frac{1}{h_b} + \frac{1}{h_t} \right) + 2N_f 7.2\mu \left(\frac{H}{g_0} \right)^3 l_f \tag{6}$$

h_b and h_t are the heights considered at the bottom and top of the structure. N_f is the number of movable fingers and l_f is the length of fingers. μ is the air viscosity that is equal to 1.87×10^{-5} (N.s)/m^2. A_s is the total area of movable part of the accelerometer and is described as:

$$A_s = l_f w_f N_f + W_p L_p \tag{7}$$

Where w_f is the width of movable fingers. Moreover, W_p and L_p are the width and length of the proof-mass, respectively.

$$L_p = \left(\frac{N_f}{2} + 1 \right) w_c + \frac{N_f}{2} w_f \tag{8}$$

Where w_c is the gap between two movable fingers and is given by:

$$w_c = 3g_0 + 2w_{ff} \tag{9}$$

Where w_{ff} is the width of fixed fingers. The mass of movable part of the accelerometer consists of the mass of proof-mass and movable fingers and is given by:

$$m = \rho H A_s \tag{10}$$

Where ρ is density.
   Using Eq. (6) and Eq. (10) N_f, l_f and the size of proof-mass will be calculated.
   The stiffness along y direction (k_y) is described as:

Table 1 Parameters used in the design of accelerometer

Parameter	a_{max} (g)	Noise density (μg/Hz)	ρ (kg/m^3)	E (GPa)	Poisson's ratio	H (μm)	T (^{0}k)	w_f (μm)	w_{ff} (μm)	w_b (μm)
Assumed values	480	110	2330	169	0.22	5	300	2	2	1

Table 2 Calculated parameters for the accelerometer

Parameter	m (μg)	b (μ(N.s)/m)	k (N/m)	Mass size (μm×μm)	l_f (μm)	N_f	l_b (μm)	A_c (m^2)
Calculated Values	0.55	9.5	0.65	170.6×252	50	40	95.3	10^{-8}

$$k_y = \frac{2}{N} \times EH\left(\frac{w_b}{l_b}\right)^3 \tag{11}$$

Where E is young's modulus, w_b is the width of each turn of the spring and l_b is the length of spring beam. Each serpentine spring has N turns. The width of the beams must be chosen in order to obtain smaller ratio of k_y to spring stiffness in z direction (k_z).

$$\frac{k_y}{k_z} = \frac{w_b^2}{H^2} \tag{12}$$

The total capacitance area (A_c) is estimated by:

$$A_c = N_f l_f H \tag{13}$$

Typical parameters assumed in this design are given in Table 1 and the calculated parameters for the accelerometer are shown in Table 2. The parameters derived here such as A_c, m, k and b will be used for system-level simulation of the accelerometer which will be explained later.

3. Open and closed loop controllers for the MEMS accelerometers

Fig. 2, is a simplified view of the MEMS accelerometer structure. The acceleration exerted on the device creates an inertial force on the proof-mass, which in turn causes the displacement of the proof-mass.
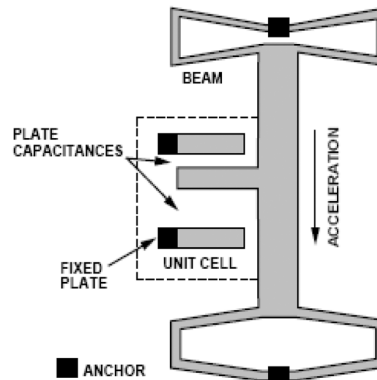

Fig. 2. Simplified view of the MEMS accelerometer under acceleration (ADXL150/ADXL250 data sheet)

In an open loop control system, the electrical output signal is directly used as the output signal of the accelerometer. Large proof-mass deflection may introduce nonlinear effects such as spring softening effect (Zhang 1998). The open loop accelerometer has limited performance in terms of bandwidth, linearity and dynamic range (Kraft 1997, Park, *et al*. 2002). To reduce these non-idealities and improve the performance a force feedback closed loop control system is normally used. The proof-mass is kept in the central position between the electrodes by applying a reset force to counter balance the accelerating force. Two electrostatic forces are superimposed on the proof-mass. The resultant force then provides a negative feedback (Park, *et al*. 2002). The dependency of the electrostatic force on the voltage is not linear. The electrostatic force is given by:

$$F_e = \frac{\varepsilon_0 A_c V^2}{4(g_0 \pm x)} \tag{14}$$

Where V is the applied voltage and ε_0 is the permittivity of the free space.

4. Conventional PID controller

The equivalent system level model for device is created using Simulink (MATLAB) software. The mathematical model consists of mechanical component, electro-mechanical sensing element, and electronic circuit controller as shown in Fig. 3. The mechanical component contains mass, damping component, and spring elements. The electro-mechanical component includes the electrostatic force. The circuit controller contains PID controller which measures the imbalance in capacitance that is converted into an output signal by a low pass filter. The transfer function and PID coefficients are chosen similar to (Park, *et al*. 2002). The operation of accelerometer can be hampered by undesirable events. For example when the applied acceleration exceeds a specified value called a_{snap}, the displacement may increase by more than the one-third of the full gap. a_{snap} can be found using Eq. (1) and is equal to 800 g for this design. A sinusoidal acceleration with 30 Hz frequency is applied to the accelerometer.

Fig. 4, shows (a) displacement and (b) output voltage for the case where input acceleration is smaller than a_{snap} as well as (c) displacement and (b) output voltage for the case where input acceleration is greater than a_{snap}. As expected the displacement increased than $g_0/3$ when input acceleration is higher than a_{snap}.
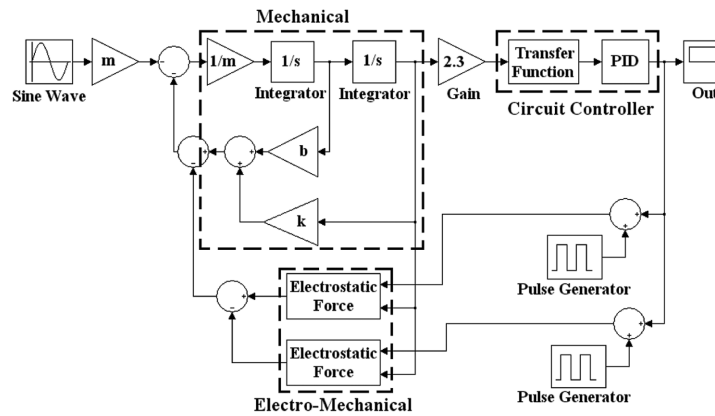

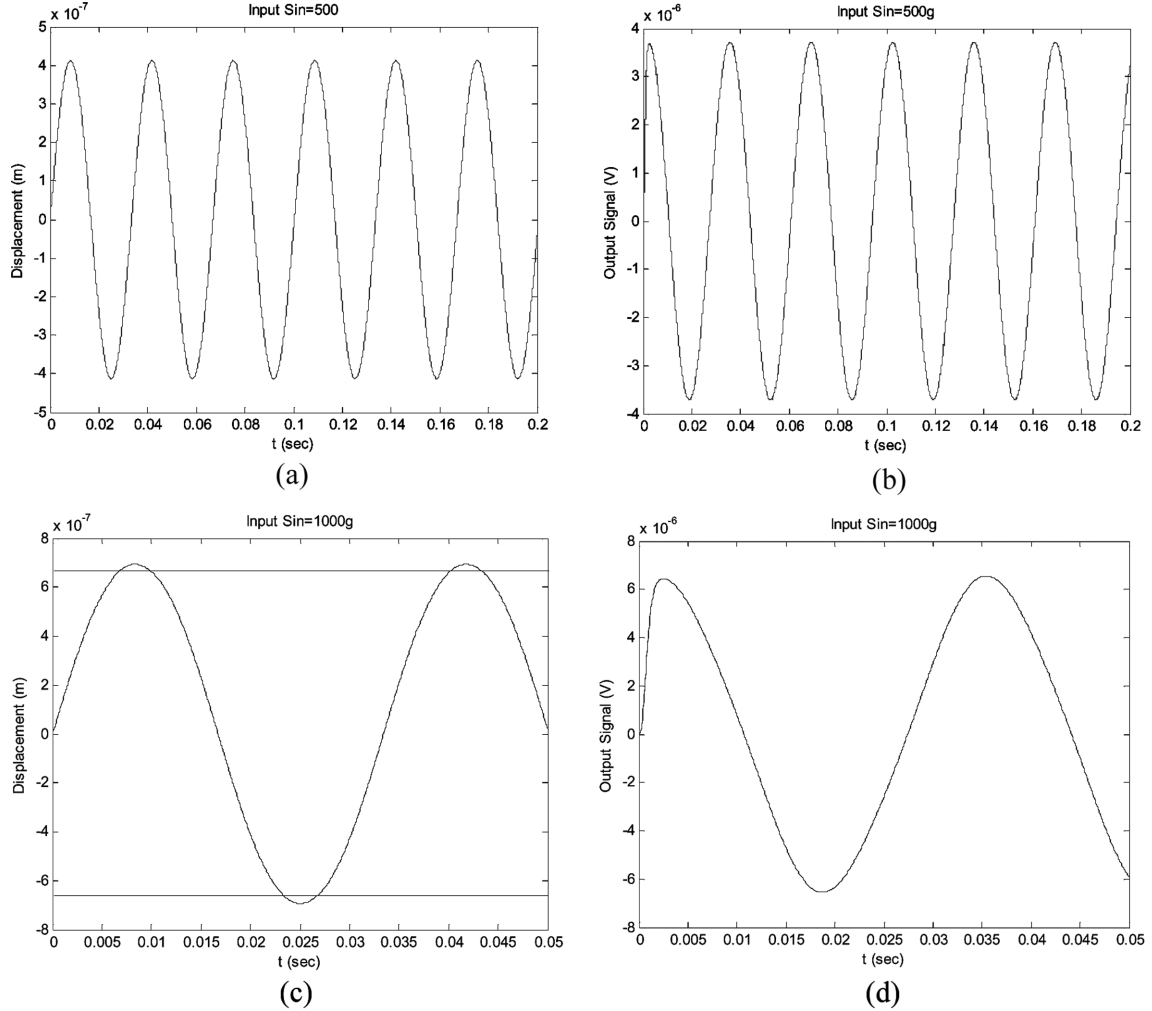Fig. 3 The system level model of device

Fig. 4 Response of the accelerometer with conventional PID controller to 30 Hz sinusoidal input acceleration. (a) displacement and (b) output voltage for amplitude of 500 g and (c) displacement and (d) output voltage for amplitude of 1000 g

The same simulations were performed for input pulses with durations of 50 ms and amplitude (a) smaller than a_{snap} (b) greater than a_{snap}, as shown in Fig. 5. It is seen from Fig. 5(b), when the input acceleration exceeds a_{snap}, the displacement exceeds the maximum allowable displacement ($g_0/3=$ 0.67 μm) and the pull-in phenomena will occur. In order to solve this problem we add a sliding-mode controller to the conventional PID closed loop system to prevent pull-in phenomena by preventing finger displacement from passing a maximum preset value.

The accelerometer's operation may be also disturbed by temperature variations and by the presence of non- idealities e.g. crack in the structure. The non- idealities induce changes in b and k and these changes can affect the accelerometer operation. We suggest an estimator which is designed based on adaptive input-output feedback linearization theory to estimate changes in b and k. The new system level model used in our simulation is shown in Fig. 6. This model is the same as conventional model except that an additional controller and an adaptive sliding mode observer are added.
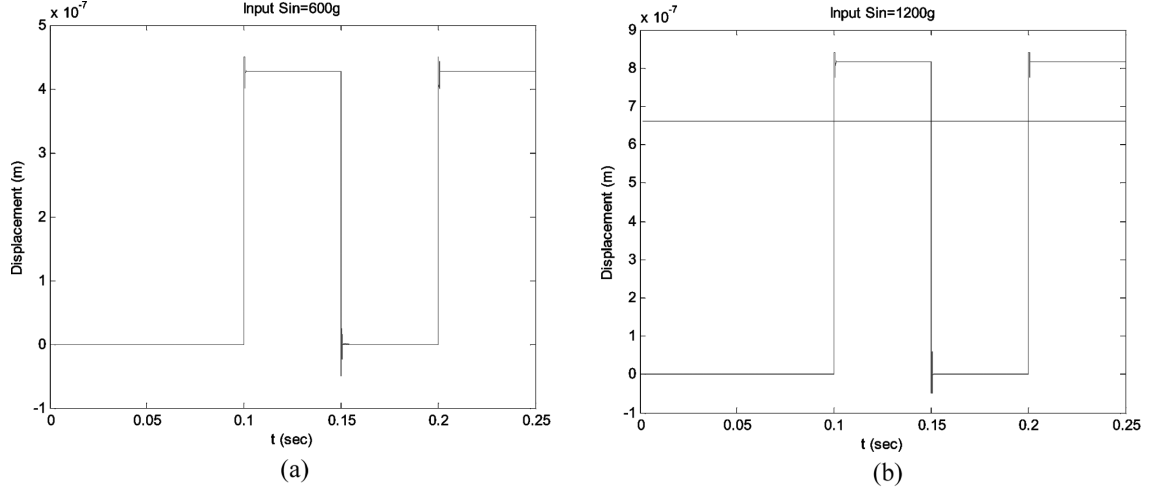
Fig. 5 The accelerometer displacement with conventional PID controller for an input pulse with duration of 50 ms and amplitude of (a) 600 g and (b) 1200 g
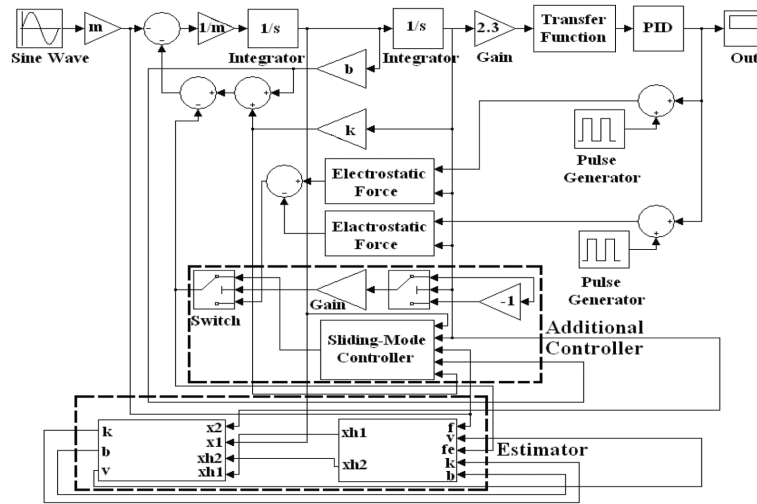

Fig. 6 The new system level model for the accelerometer

5. Sliding-mode controller

When the input acceleration exceeds a_{snap}, the displacement exceeds the maximum allowable displacement. So, an additional sliding-mode controller is used to alleviate the pull-in effect. This sliding-mode controller is designed to work in parallel with conventional controller. When displacement reaches near the maximum allowed point ($g_0/3$), this controller is switched on to prevent the finger displacement from exceeding a maximum preset value.

A sinusoidal acceleration with 30 Hz frequency is applied to the accelerometer. Fig. 7, shows (a) displacement and (b) output voltage for the case where input acceleration is smaller than a_{snap}, as expected the controller is not functioning in this case thus the displacement and output voltage exactly match those shown in Fig. 4 (a) and (b). Fig. 7 (c) shows the displacement and (d) output voltage for the
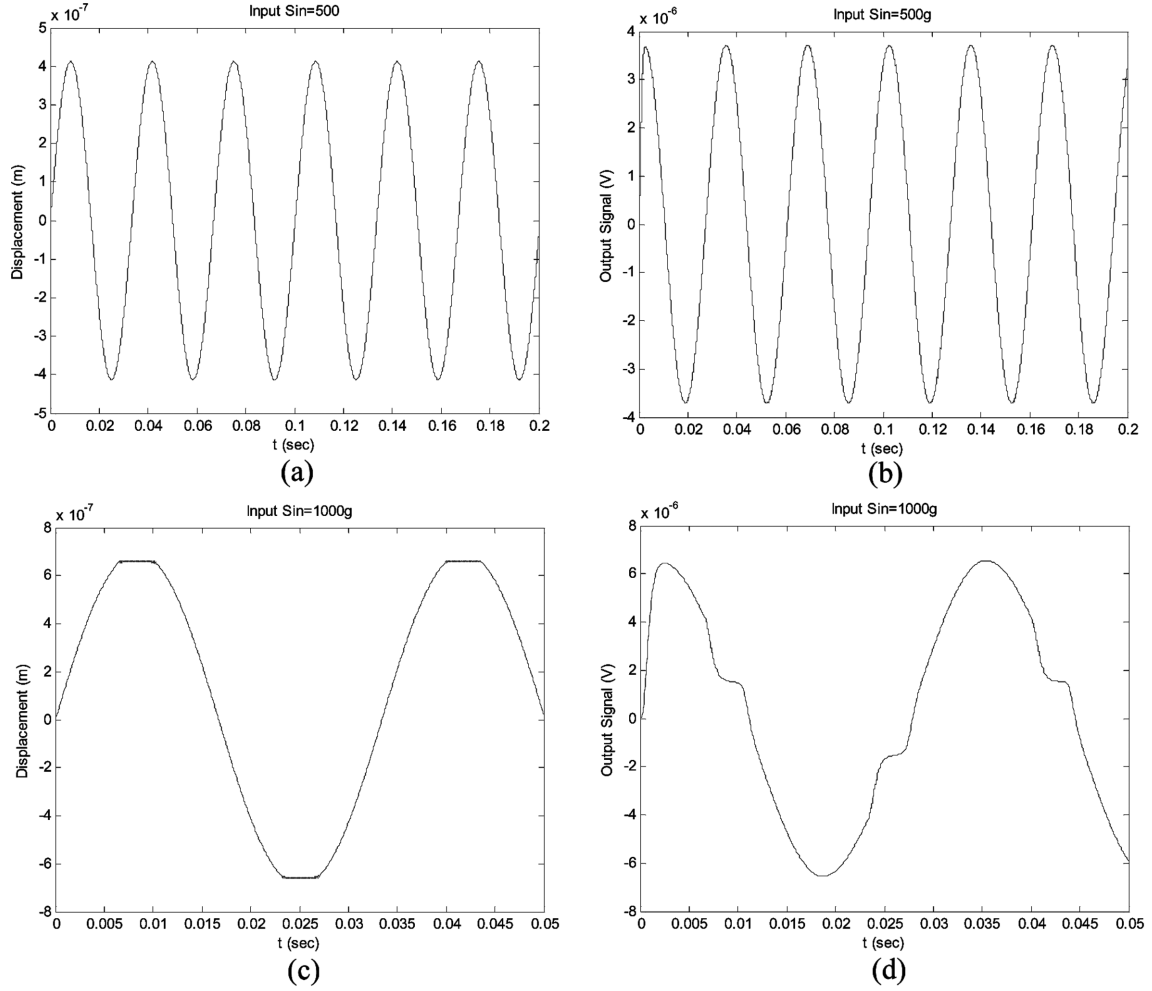
Fig. 7 Response of the accelerometer with sliding mode controller to 30 Hz sinusoidal input acceleration. (a) displacement and (b) output voltage for amplitude of 500 g, (c) displacement and (d) output voltage for amplitude of 1000 g

case where input acceleration is greater than a_{snap}, as expected the controller is functioning in this case consequently the displacement stays within the maximum allowable range and pull-in phenomena is prevented.

In Fig. 8, another mechanical test is carried out to evaluate the performance of the proposed method against a pulse train acceleration with 50 ms duration and amplitude of (a) 600 g and (b) 1200 g. As seen in Fig. 8(a) input acceleration has not caused displacement to exceed $g_0/3$, thus the sliding-mode controller is not functioning. However in Fig. 8(b) the sliding-mode controller is functioning since in this case the input acceleration is greater than a_{snap} and has caused an out of range displacement.

The distortion of the output signal is due to inserting the additional force that is caused by the sliding-mode controller when the displacement passes the maximum preset value. In other words, when the applied acceleration to the accelerometer is large enough to force it to pass the maximum preset value,
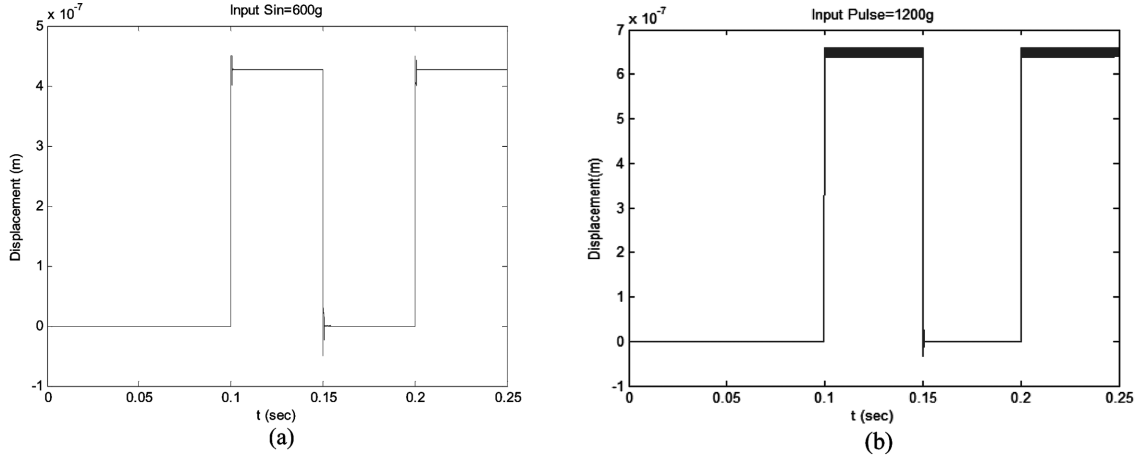
Fig. 8 The accelerometer displacement with sliding-mode controller for an input pulse with duration of 50 ms and amplitude of (a) 600 g and (b) 1200 g

the controller maintains the displacement in the maximum threshold. This fact is depicted in Fig. 7(c) and Fig. 8(b). Therefore, in this situation, due to the relation between displacement and output signal, the output signal is distorted.

6. Sliding-mode design of closed loop system

In this section, design of a hybrid controller is presented. This controller is designed based on combination of the conventional PID controller with sliding-mode controller. In order to model the device system model, a mathematical model is studied for sensing element and incorporated into system level. The corresponding differential equation is:

$$m\ddot{x} + b\dot{x} + kx = F_e - ma_{in}(t) \tag{15}$$

Where m is mass, k is spring stiffness and b is damping factor. Moreover a_{in} is input acceleration.

We may define this equation as:

$$\dot{x}_1 = x_2$$
$$\dot{x}_2 = -\frac{b}{m}x_2 - \frac{k}{m}x_1 + \frac{F_e}{m} - a_{in}(t) \tag{16}$$

Let:

$$z_1 = x_1$$
$$z_2 = x_2 \tag{17}$$

And:

$$f_2(z_1, z_2) = -\frac{b}{m}z_2 - \frac{k}{m}z_1 - a_{in}$$

$$\hat{u} = \frac{Fe}{m} \tag{18}$$

The dynamical model of system Eq. (15) becomes as follows:

$$\dot{z}_1 = z_2$$
$$\dot{z}_2 = f_2(z_1, z_2) + \hat{u} \tag{19}$$

The reference model is designed in a linear form as:

$$\begin{bmatrix} \dot{z}_{m1} \\ \dot{z}_{m2} \end{bmatrix} = \begin{bmatrix} 0 & a_{m2} \\ a_{m3} & a_{m4} \end{bmatrix}\begin{bmatrix} x_1 \\ x_2 \end{bmatrix} + \begin{bmatrix} a_{m5} & 0 \\ 0 & a_{m6} \end{bmatrix}\begin{bmatrix} x_1^* \\ x_2^* \end{bmatrix}$$

$$x_1^* = x_2^* = 0$$

$$a_{m2} = 1, a_{m3} = -\frac{k}{m}, a_{m4} = -\frac{b}{m} \tag{20}$$

Furthermore we define the tracking errors between plant and reference model as:

$$e_z = [z_1 - z_{m1} \ z_2 - z_{m2}]^T = [e_{z1} \ e_{z2}]^T \tag{21}$$

The error dynamics are derived as follows:

$$\dot{e}_z = A(x) + B(x)\bar{u}$$

$$A(x) = \begin{bmatrix} e_{z2} \\ f_2(z_1, z_2) \end{bmatrix}, B(x) = \begin{bmatrix} 0 \\ 1 \end{bmatrix} \tag{22}$$

According to Eq. (22), the sliding surface is designed as:

$$\sigma(e_z) = Se_z(x) \tag{23}$$

Where $S \in \Re^{1 \times 2}$ is a constant linear matrix and inverse of $SB(x)$ must exist. It follows that $\det(SB(x)) \neq 0$ for all x. Here the dynamics of the sliding surface as a specified form is designed as:

$$\dot{\sigma} = S\dot{e}_z = SA(x) + SB\bar{u} = -Q\text{sgn}(\sigma) - K\sigma$$

$$\text{sgn}(\sigma) = \begin{cases} 1 & \text{as} \ \sigma > 0 \\ -1 & \text{as} \ \sigma < 0 \end{cases} \tag{24}$$

Where $Q > 0$ and $K > 0$.

Then, the controller in terms of $\bar{u}$ can be described as:

$$\bar{u} = -(SB)^{-1}[SA(x) + Q\text{sgn}(\sigma) + K\sigma] \tag{25}$$

Using the proposed controller the desired goal of sliding-mode control system which is eliminating the error, is achieved.

We will now show that with the developed nonlinear sliding surface Eq. (23), the reaching condition $\sigma\dot{\sigma} < 0$ is satisfied, and the controlled system Eq. (25) will be stabilized.

Multiplying σ on both sides of the Eq. (24), we obtain:

$$\sigma\dot{\sigma} = -Q\sigma\mathrm{sgn}(\sigma) - K\sigma^2 = -Q|\sigma| - K\sigma^2 < 0 \tag{26}$$

From the above analysis, it is evident that reaching condition is guaranteed.

7. Adaptive nonlinear observer

The estimator is designed based on a nonlinear discipline called adaptive input-output feedback linearization theory (Krstic, *et al.* 1995), to detect the spring stiffness and the damping factor of the MEMS accelerometer in an online fashion. This observer has the capability of estimating changes both in k and b either in presence or absence of the feedback controller. As mentioned before both temperature variations and also the presence of non- idealities in the accelerometer's structure results in variation in k and b.

Consider for example variation in k (Δk) caused by a crack with dimensions as specified in Fig. 9(a). The Finite Element Method is carried using ANSYS (ANSYS software). For the static analysis 1 g constant acceleration is applied in y direction. The Von Mises stress contour for the accelerometer structure shows that the stress in the proof mass and fingers is uniform and that the maximum stress occurs in the folded parts of the springs. The crack created at different positions is shown in Fig. 9(b). Fig. 10 shows the variation of natural frequency versus crack position. The results show that if the crack is positioned at places with higher stress it would produce a higher natural frequency. Changes in natural frequency resulted in a maximum Δk of 0.01 N/m using Eq. (5) and different frequencies shown in Fig. 10.

As another example, the impact of temperature on b is considered. Damping factor is proportional to viscosity (μ). Using Sutherland formula, viscosity is described as:

$$\dot{\mu}_0 = \mu_0 \frac{T_0 + C}{T + C}\left(\frac{T}{T_0}\right)^{\frac{3}{2}} \tag{27}$$

Where T_0 and μ_0 are reference temperature and viscosity, respectively. C is Sutherland's constant. Moreover, $\dot{\mu}_0$ is viscosity at operating temperature (T). These constants for air are:
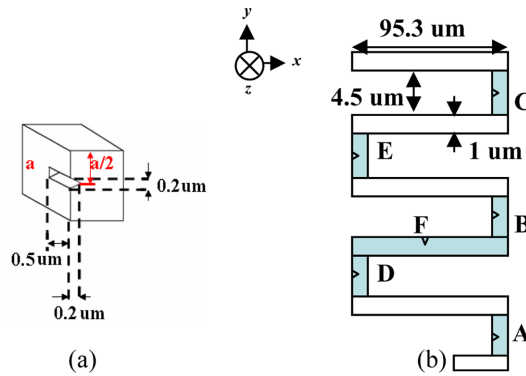

Fig. 9 (a) Crack's dimension (b) different points at which the crack was positioned
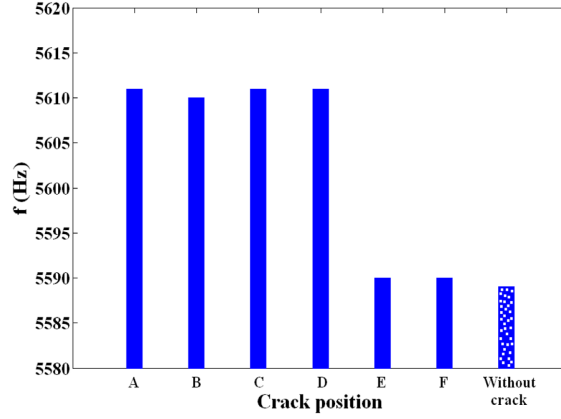
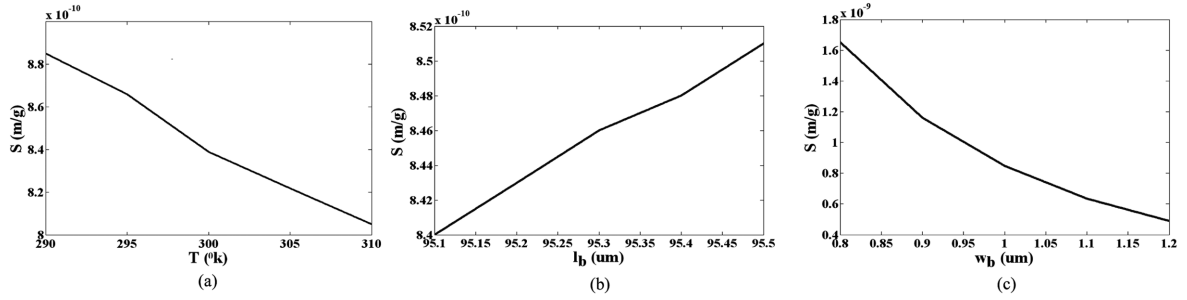Fig. 10 The variation of natural frequency versus crack's position

Fig. 11 Sensitivity changes versus variations in (a) temperature and (b) changes in the length of spring dimension (c) changes in the width of spring

$$C = 120^0\text{K}, \ T_0 = 291.15^0\text{K}, \ \mu_0 = 18.27 \times 10^{-6} \text{ Pa.s.}$$

The changes in damping factor (Δb) due to 2 degrees increase in temperature is found to be 0.04 ($\mu N.s$)/m using Eq. (6) and Eq. (27).
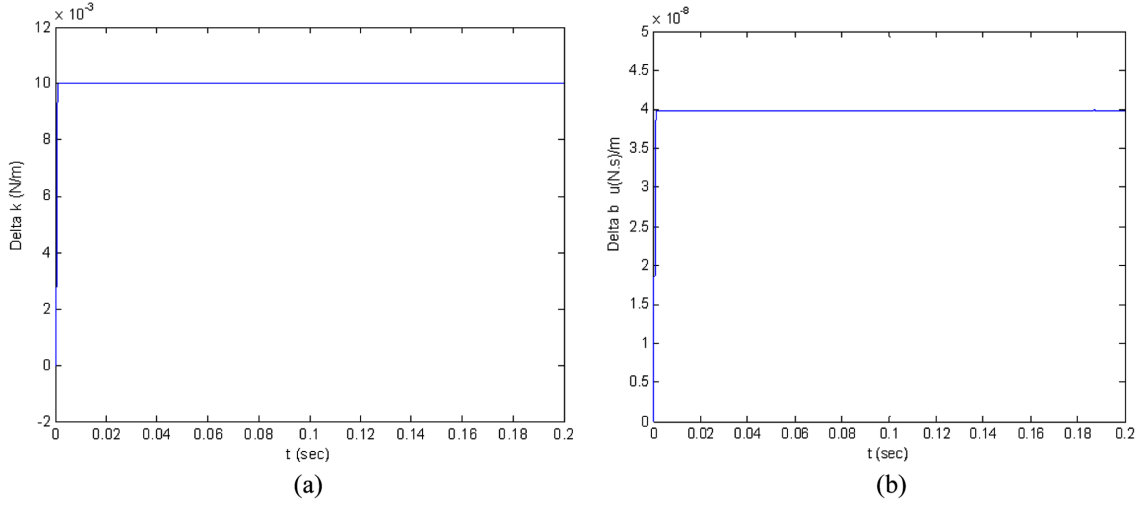
We define sensitivity as x/a. Changes in sensitivity versus (a) temperature variations as well as changes in (b) the length of spring and (c) the width of spring are shown in Fig. 11. These results show the degree by which changes in b and k can affect the operation of accelerometer.

The actual values of k (k_a) and b (b_a) are 0.66 N/m and 9.54 ($\mu N.s$)/m by adding $\Delta k = 0.01$ N/m and $\Delta b = 0.04$ ($\mu N.s$)/m to k and b that are derived in section 2. Δk and Δb were used in order to predict the operation of the observer against these changes. The results for Δk and Δb are shown in Fig. 12. As can be seen from Fig. 12, the estimator correctly estimates the difference between actual and nominal parameters.

8. Design of adaptive input-output feedback linearization observer

For the adaptive Input-Output Feedback Linearization design of the observer (estimator) the notation is simplified by following definitions:

$$y_1 = x_1$$

Fig. 12 (a) Δk and (b) Δb associated with the estimator

$$y_2 = x_2$$

$$a_2 = \frac{b}{m}$$

$$a_1 = \frac{k}{m} \tag{28}$$

The accelerometer equations are:

$$\begin{bmatrix} \dot{x}_1 \\ \dot{x}_2 \end{bmatrix} = \begin{bmatrix} 0 & 1 \\ -a_1 & -a_2 \end{bmatrix} \begin{bmatrix} x_1 \\ x_2 \end{bmatrix} + \begin{bmatrix} 0 \\ \frac{F_e}{m} \end{bmatrix} - \begin{bmatrix} 0 \\ 1 \end{bmatrix} a_{in}$$

$$y_1 = x_1$$

$$y_2 = x_2 \tag{29}$$

Because the outputs y_1, y_2 are measurable, the prediction model for the Input-Output Feedback Linearization observer design is chosen to be:

$$\begin{bmatrix} \dot{\hat{x}}_1 \\ \dot{\hat{x}}_2 \end{bmatrix} = \begin{bmatrix} 0 & 1 \\ -\hat{a}_1 & -\hat{a}_2 \end{bmatrix} \begin{bmatrix} y_1 \\ y_2 \end{bmatrix} + \begin{bmatrix} 0 \\ \frac{F_e}{m} \end{bmatrix} - \begin{bmatrix} 0 \\ 1 \end{bmatrix} a_{in} \begin{bmatrix} 0 \\ v \end{bmatrix}$$

$$\hat{y}_1 = \hat{x}_1$$

$$\hat{y}_2 = \hat{x}_2 \tag{30}$$

Where v is the control input. This input is to be designed by the Input-Output Feedback Linearization method.

The prediction errors are:

$$\tilde{x}_1 = \hat{x}_1 - x_1$$
$$\tilde{x}_2 = \hat{x}_2 - x_2$$
$$\tilde{a}_1 = \hat{a}_1 - a_1$$
$$\tilde{a}_2 = \hat{a}_2 - a_2 \tag{31}$$

The dynamical equations for Eq. (31) are then given by:

$$\begin{bmatrix} \dot{\tilde{x}}_1 \\ \dot{\tilde{x}}_2 \end{bmatrix} = \begin{bmatrix} 0 & 1 \\ -\tilde{a}_1 & -\tilde{a}_2 \end{bmatrix} \begin{bmatrix} y_1 \\ y_2 \end{bmatrix} + \begin{bmatrix} 0 & 1 \\ -\hat{a}_1 & -\hat{a}_2 \end{bmatrix} \begin{bmatrix} \tilde{y}_1 \\ \tilde{y}_2 \end{bmatrix} + \begin{bmatrix} 0 \\ v \end{bmatrix}$$

$$\tilde{y}_1 = \tilde{x}_1 = \hat{y}_1 - y_1 = 0$$
$$\tilde{y}_2 = \tilde{x}_2 = \hat{y}_2 - y_2 = 0 \tag{32}$$

The second equation is obtained for:

$$v = -c_1 \tilde{x}_2 + \hat{a}_1 \tilde{y}_1 + \hat{a}_2 \tilde{y}_2 \tag{33}$$

In this equation, c_1 is a positive parameter.

8.1. Stability analysis

The obtained equations give the error dynamics for the field observer as:

$$\dot{\tilde{x}}_1 = 0$$

$$\dot{\tilde{x}}_2 = -\tilde{a}_1 x_1 - \tilde{a}_2 x_2 - c_1 \tilde{x}_2 \tag{34}$$

This system has equilibrium at $\tilde{x}_1 = \tilde{x}_2 = 0$.
 Furthermore the derivative of the Lyapanouv function candidate is as follows:

$$V = \frac{1}{2} \left\{ \|\tilde{x}_1\|^2 + \|\tilde{x}_2\|^2 + \frac{1}{\gamma_1} \tilde{a}_1^2 + \frac{1}{\gamma_2} \tilde{a}_2^2 \right\} \tag{35}$$

Where $\gamma_1 > 0, \gamma_2 > 0$.
 The time derivative of V is found as:

$$\dot{V} = -c_1 \|\tilde{x}_2\|^2 + \tilde{a}_1 \left\{ \frac{1}{\gamma_1} \frac{d\tilde{a}_1}{dt} - (\tilde{x}_2 x_1) \right\} + \tilde{a}_2 \left\{ \frac{1}{\gamma_2} \frac{d\tilde{a}_2}{dt} - (\tilde{x}_2 x_2) \right\} \tag{36}$$

For $\dot{V} < 0$, we must consider:

$$\frac{1}{\gamma_1}\frac{d\tilde{a}_1}{dt} - real(\tilde{x}_2 x_1) = \frac{1}{\gamma_2}\frac{d\tilde{a}_2}{dt} - real(\tilde{x}_2 x_2) = 0 \qquad (37)$$

Finally, adaptation laws obtained as:

$$\dot{\tilde{a}}_1 = \gamma_1 real(\tilde{x}_2 x_1)$$

$$\dot{\tilde{a}}_2 = \gamma_2 real(\tilde{x}_2 x_2) \qquad (38)$$

9. Conclusion

In this paper a hybrid controller for closed loop feedback of MEMS accelerometer is presented. This hybrid controller is designed based on a combination of a sliding-mode controller and a PID controller. The advantage of this controller is preventing displacement from exceeding a maximum preset value. The PID controller is unable to perform this task. Implementing sliding-mode controller thus can extend the working range of accelerometer to a much larger value. Moreover a new estimator for the conventional capacitive MEMS accelerometer was presented. This scheme is realized by adding an adaptive nonlinear observer to a conventional PID closed loop system. The estimator was used for online estimation of the parameter variations for MEMS accelerometers and provided the capability of self testing for the system. Simulation analysis confirms the effectiveness and validity of the presented method.

References

ADXL150/ADXL250 data sheet, Analog Devices.

ANSYS software, Version. 10.

Chowdhury, S., Ahmadi, M. and Miller, W.C. (2005), "Pull-In Voltage calculations for MEMS Sensors with Cantilevered Beams", *The 3rd Int. IEEE-NEWCAS Conf.*, 143-146.

Edvards, C. and Spurgeon, S.K. (1998), *Sliding Mode Control*, TAYLOR & FRANCIS.

Kraft, M. (1997), *Closed Loop Digital Accelerometer Employing Oversampling Conversion*, Ph.D. thesis, Coventry University, School of Engineering, UK.

Krstic, M., Kanelleskapoulas, I. and Kokotovic, P. (1995), *Nonlinear and Adaptive Control design*, New York, John Wiley and Sons. Inc.

Lobontiu, N. and Garcia, E. (2005), *Mechanics of Microelectromechanical Systems*, Springer Science + Business Media, Inc.

Luo, H., Zhang, G., Carley, L.R. and Fedder, G.K. (2002), "A Post-CMOS Micromachined Lateral Accelerometer", *J. Microelectromech. Syst.*, **11**,188-195.

Lyshvitz, S.E. and Lyshvitz, M.A. (2000), "Analysis, Dynamics, and Control of Micro-Electromechanical Systems", *Proc. of American Control Conf.,* Chicago, 3091-3095.

Park, K., Pochiraju, K. and Varadan, V.K. (2002), "A hierarchical model for MEMS device performance simulation", *SPIE Proc. Series*, **4700**,135-146.

Park, S. and Horowitz, R. (2003), "Adaptive Control for the Conventional Mode of Operation of MEMS Gyroscopes", *J. Microelectromech. Syst.*, **12**, 101-108.

Slotine, J. and Jacques, E. (1991), *Applied Nonlinear Control*, Prentice-Hall.

Spooner, J.T., Maggiore, M., Ordonez, R. and Passino, K.M. (2002), *Stable Adaptive Control and Estimation for Nonlinear Systems*, New York, John Wiley and Sons. Inc.

System Planning Corporation (1994), *Micro Electro Mechanical Systems (MEMS) an SPC market study.*

Vishal, G. (2000), *Approaches to Synthesis of a CMOS Accelerometer*, M.S. thesis, Carnegie Mellon University.
Yazdi, N., Ayazi, F. and Najafi, K. (1998) "Micromachined Inertial Sensors", *Proc. of the IEEE*, **86**, 1640-1659.
Zhang, G. (1998), *Design and Simulation of CMOS-MEMS accelerometer*, Project Report, Carnegie Mellon University.
Zhu, G., Penet, J. and Saydy, L. (2006), "Robust Control of an Electrostatically Actuated MEMS in the Presence of Parasitics and Parametric Uncertainties", *Proc. of the 2006 American Control Conf.*, Minneapolis, 1233-1238.

JK